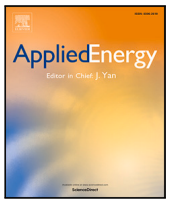
Applied Energy 378 (2025) 124725



Contents lists available at ScienceDirect

Applied Energy

journal homepage: www.elsevier.com/locate/apenergy





Numerical Modeling of Metal Hydride-Phase Change Material Hydrogen Storage Systems with Increased Heat Exchange surface area ☆

Marco Maggini [a], Andrea L. Facci [a,*], Giacomo Falcucci [b,c], Stefano Ubertini [a]

[a] Department of Economics, Engineering, Society and Business Organization, University of Tuscia, 01100 Viterbo, Italy
[b] Department of Enterprise Engineering Mario Lucertini, University of Rome Tor Vergata, Via del Politecnico 1, 00133 Rome, Italy
[c] Department of Physics, Harvard University, Cambridge, MA 02138, USA

ARTICLE INFO

Keywords:
Hydrogen technologies
Energy systems
Hydrogen storage
Phase change material
Metal hydrides

ABSTRACT

Coupling Metal Hydrides (MH) with Phase Change Materials (PCM) provides a promising way of storing hydrogen without using any active systems to control the MH temperature during cycling. In this study, we perform numerical assessments on the performance of cylindrical MH-PCM storage systems with varying geometrical configurations. We investigate the ab/desorption kinetics in a straight cylindrical geometry (case A), where the PCM surrounds the MH. Its cycle time and gravimetric density for the absorption of 1.04 kWh are 2,200 s and 0.30%. We then investigate two improved configurations, namely the addition of fins to the external surface of the MH and within the PCM domain (case B), and the containment of the MH powder into a helix-shaped tube immersed in the PCM (case C). Number and thickness of fins are also varied to assess their impact. Compared to case A, the helix-shaped design is 49% and 40% faster in absorption and desorption, respectively, whereas the finned geometry is 28.9% and 30% faster. The gravimetric density is 0.27% and 0.62% in case B and C, respectively.

1. Introduction

The intermittent nature of RES poses multiple challenges as for their fully fledged implementation, mainly related to the stability and the operations of the power systems [1,2]. Therefore, among other significant solutions, the large scale implementation of an effective and efficient energy storage system is pivotal to overcome the above-mentioned issues [3–5].

Hydrogen has shown good potential as energy storage medium [6]. Potentially carbon neutral and secure energy is fundamental in many different sectors, in particular in the hard-to-abate ones, where hydrogen might play a significant role in the next future [7–11]. In this context, it is apparent how an efficient, compact, and cost-effective hydrogen storage option is needed [12]. The main hydrogen storage methods are gas, liquid, and solid storage [13].

Metal Hydride hydrogen storage is a promising option [14], pertaining to the solid-state methods. Compared to gas and liquid storage, MHs are safe, have higher volumetric density, lower operating pressure and temperatures [15–18]. $LaNi_5$, which is used in this work, and its hydride also present low flammability, explosibility, and combustibility risks. The spontaneous ignition is difficult to accomplish and the resistance to shocks and impacts is relatively high [19]. This makes $LaNi_5$ relatively safe to handle and use. However, MH technologies do not fulfill the criteria for a practical hydrogen economy yet [12]. This is due to the slow kinetics of reaction and the difficulty in controlling MH temperatures during hydrogenation and de-hydrogenation. More specifically, the hydrogenation (or hydrogen absorption) and dehydrogenation (or hydrogen desorption) to/from MH are exothermic and endothermic processes, respectively. The reaction rate (mol_{H_2} reacting per unit time) is maximized if we manage to control the MH temperature [20]. This means disposing of the absorption heat, and providing the desorption heat. Thus, thermal control and management is pivotal to enhance MH performance [21,22]. To deal with such issue, current research focuses on: (i) improving the effective thermal conductivity of the MH powder (e.g., using Expanded Natural Graphite inclusions); (ii) designing high-efficiency internal/external heat exchangers; (iii) alternative methods (e.g., Phase Change Materials (PCMs) utilization).

The latter is an efficient passive solution, which does not need any additional active systems (e.g., heat exchangers or heat pipes). Specifically, the Phase Change Material works as a thermal energy storage

☆ The short version of the paper was presented at ICAE2023, Doha, Qatar, Dec 3–5, 2023. This paper is a substantial extension of the short version of the conference paper.

* Corresponding author.
E-mail address: andrea.facci@unitus.it (A.L. Facci).

https://doi.org/10.1016/j.apenergy.2024.124725
Received 28 June 2024; Received in revised form 12 September 2024; Accepted 14 October 2024
Available online 26 October 2024
0306-2619/© 2024 The Authors. Published by Elsevier Ltd. This is an open access article under the CC BY license (http://creativecommons.org/licenses/by/4.0/).

unit, transferring heat almost at constant temperature by alternatively melting and solidifying [23–25]. The choice of an appropriate PCM and the optimization of its quantity are essential to ensure efficient heat transfer and fast hydrogen charge and discharge rates [26]. In particular, the melting enthalpy should be equal or larger than the reaction enthalpy of MH [20], and the phase change temperature must be between the ab/desorption equilibrium temperatures at a given working pressure [27]. One significant disadvantage of employing PCMs as passive temperature controllers is their low thermal conductivity [28]. Currently, various research investigates distinct aspects of MH-PCM coupling, MH-heat exchanger systems, and PCM-based thermal storage units.

Dong et al. [29] proposed a novel MH-based reactor with honeycomb fins and PCM to enhance heat transfer. The authors demonstrate that, in comparison with the reactor without fins, the ab-desorption rate is increased while the storage density is decreased. They also show that the storage cycle is reduced by 84% if the reactor is filled with sandwich PCM, compared to the reactor with PCM on the periphery of the honeycomb. A. Jemni et al. [30] developed a 2D mathematical model for heat and mass transfer in a metal hydride reactor. The reactor is cylindrical and a high temperature fluid is considered in contact with the base and lateral surfaces. The heat transfer fluid is constantly at 313 K. The reactor is filled with $LaNi_5$, initially at 290 K, and the inlet pressure is 10 bar. The authors compare results for different canister aspect ratios $\mathcal{R} = \frac{\text{length}}{\text{radius}}$ and operating conditions (fluid temperature and hydrogen pressure). They conclude that, for $\mathcal{R} \ll 2.5$ or $\mathcal{R} \gg 2.5$, the 2D effects can be neglected without significant discrepancy. Most importantly, the results show that the heat transport via convection inside the MH can be neglected, because an error < 1% is induced. This allows to simplify the mathematical models.

Yao et al. [31] used a modified numerical model to characterize the absorption and desorption heat and mass transfer of MH-PCM tanks. The modified model accounts for a continuous absorption/desorption process to better describe actual experiments. The model is 2D and considers the pressure gradient within the canister to be negligible. Five scenarios are studied to characterize the process behavior: case 1, 2, and 3 employ transversal fins which are connected to the MH, to the PCM, and through the PCM respectively; case 4 and 5 use Expanded Graphite (EG) in MH and in both MH and PCM respectively. Cases 2 and 5 present the slowest and fastest process, respectively. The authors also study the coupling of the recommended option (case 5) with a PEM-Fuel Cell to provide a practical application. The authors conclude that adding EG to MH and PCM is better than adding fins in the reactor, being at least 25% more efficient than case 1. We comment that such an option, albeit efficient, reduce the volume energy density of the storage system. Garrison et al. [32] made a comparison between longitudinal and transversal finned metal hydride reactors. A HTF flows through the central artery, to which the fins are attached. Two issues are underlined with respect to the transversal fins: (a) difficulty of automatized assembly, useful for reducing costs; (b) the heat transfer surface is reduced by proceeding from the fins tips to the reactor axis. The 3D analysis via COMSOL demonstrates that the longitudinal fins are slightly better at enhancing the heat transfer between MH and HTF. Zhang et al. [33] compared several layouts of longitudinal finned heat exchangers inserted into the MH. $LaNi_5$ is used as hydride powder. Specifically, straight fins, fan-shaped fins and quadratic curve-shaped fins are compared. The quadratic curve-shaped fins exhibits comparatively lower temperatures at the same radius ratio, implying good heat transfer. Then, circumferential fins are added to the optimized layout. It is noteworthy that, while adding fins enhances greatly the reaction, the comparison between different layouts of fins yields almost insignificant differences. Nyamsi et al. [34] investigated the charging/discharging behavior of a $LaNi_5$ packed metal hydride reactor with surrounding RT35 PCM using a 2D mathematical model. Transversal fins protrude from the MH inside the PCM. Such a system proves sufficiently good for stationary applications (e.g., PEM-FCs). Among various layouts concerning fins thickness, length, and number, the authors narrow down to a few optimal configurations. Then, they pick the best solution through an optimization test in terms of time of charge and discharge. They provide geometrical values for optimized fins, and also compare many configurations which differ in PCM thermo-physical properties.

Krsatev et al. [35] condenses available literature data up to 2023 on MH-PCM storage systems to show that is generally challenging to simultaneously achieve power/capacity ratios and volumetric storage efficiencies of 0.75 kW/kWh and 15 kg_{H_2}/m^3, respectively.

This work fits into this scenario, aiding in finding new and better solutions to increase the hydrogen storage efficiency in solid-state systems. In particular, it proposes a novel helix-shaped geometry which exhibits lower cycle times (and thus higher ab-desorption powers) compared to traditional cylindrical canisters with the same volumetric density. It also includes a sensitivity analysis to the geometry and number of longitudinal fins applied to the MH external surface, to make a comparison with the newly proposed design.

The paper is organized as follows. In Section 2 we describe the system, the mathematical model, the domains discretization, and the heat exchange model. Results for the absorption and desorption processes are presented and discussed in Section 3. Finally, we draw the conclusions in Section 4.

2. Methodology

2.1. System description

The present work investigates three different geometries of a MH-PCM systems (see Fig. 1): (i) case A is the base cylindrical design; (ii) case B is the finned geometry; (iii) case C is an helix geometry.

We select $LaNi_5$ as MH and we assume a porosity $\xi = 0.5$. The canister length $\mathcal{L}$ and diameter $d = 2b_1$ are based on the results of a comprehensive non-dimensional analysis, previously conducted by the authors (cfr. [36]). The investigation allowed to find a recommended configuration in terms of geometrical and thermo-physical properties of the storage system. Specifically, a canister with an aspect ratio $\mathcal{L}/d = 50$, Prandtl number $Pr = 4.5$, $\frac{k_{\text{PCM}}}{k_{\text{MH}}} = 0.45$, $\frac{c_{p,\text{PCM}}}{c_{p,\text{MH}}} = 5.25$, and $\frac{\rho_{\text{PCM}}}{\rho_{\text{MH}}} = 0.28$ is selected, where k, c_p, and ρ are the thermal conductivity, specific heat, and density, respectively. Therefore, $\mathcal{L}$ is 1.27 m and d is 2.54 cm, or 1 inch. The MH is surrounded by an external cylindrical jacket of PCM ($LiNO_3$ - $3H_2O$) of radius b_2 as shown in Fig. 1.A. The external surfaces are perfectly insulated (see [37]) while the hydrogen gas diffuses through the inner MH space by means of a central porous artery of radius $b_0 = 2.5$ mm, which pierces the MH along its longitudinal axis. This facilitates the gas diffusion, which mainly takes place in the radial direction. Therefore, the MH internal volume is $6.19\times10^{-4}\,m^3$. The mass of MH is 2.25 kg (given $\xi = 0.5$). Such a system can store 31.2 g of hydrogen, or 1.04 kWh, in the form of $LaNi_5H_6$.

The canister is charged at $p^a_{H_2} = 30$ bar and discharged at $p^d_{H_2} = 1$ bar. The melting point of $LiNO_3$ - $3H_2O$ ($T_m = 303$ K) matches the equilibrium temperatures in absorption and desorption of $LaNi_5$ at the selected pressures, thus allowing for a passive control of the MH temperature. Thus, the PCM melts during absorption by disposing of the hydrogenation heat, whereas it solidifies in desorption by providing the desorption heat to the MH.

Referring to the geometries of Fig. 1, the longitudinal Aluminum fins in case B protrude from the MH external surface into the PCM, with a length equal to $b_2 - b_1 = 20$ mm. A sensitivity analysis is made over the fins thickness and number, so that 11 sub-cases are investigated. Case C is a novel helix geometry, where the MH powder is contained in a helix-shaped tube immersed in the PCM. The helix has pitch h_p, spiral diameter h_D, and strand diameter h_d.

For consistency, the mass of MH (and, thus, of hydrogen stored) is the same in each case.

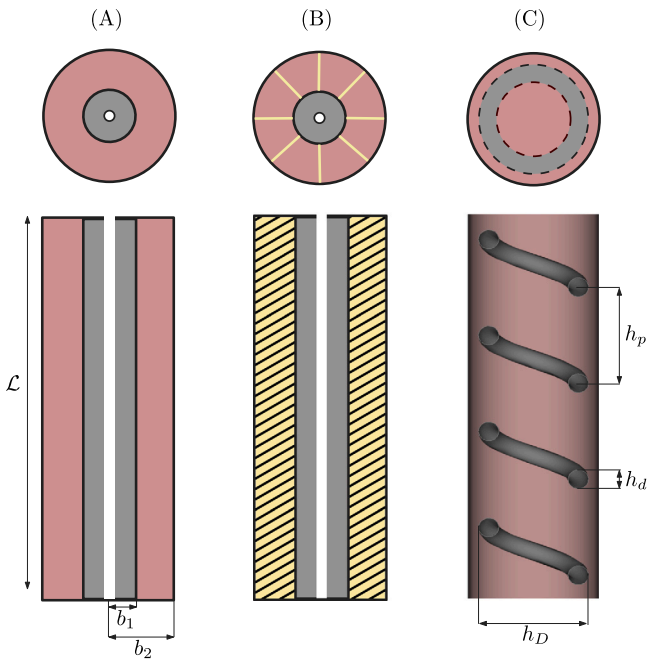


Fig. 1. Schematics of cases A (base cylinder), B (finned cylinder), and C (helix).

2.2. Mathematical modeling

The following hypotheses were considered for the mathematical model: (i) hydrogen is treated as an ideal gas, i.e., $p_{H_2} = \frac{m_{H_2} RT}{V}$ (see for instance [38]); (ii) the porous MH is homogeneous (see for instance [39]); (iii) the hydrogen inlet/outlet pressure is constant during uptake and release, respectively (see for instance [40]); (iv) the thermo-physical properties of MH and PCM do not change with temperature [41]; (v) the gas pressure inside the canister is uniform [38]; (vi) the gas and the MH are in local thermal equilibrium, i.e., $T_{MH} = T_{H_2}$ locally.

Further consideration is needed for the assumption of no appreciable pressure gradient inside the vessel (assumption (v)). Chaise et al. [38] have demonstrated that such an assumption is valid whenever the newly introduced non-dimensional number

$$N = \frac{k_e \cdot M_{H_2} \cdot L_{gas}^2 \cdot \mu_{H_2}}{\frac{\partial P_{eq}}{\partial T} \cdot \Delta H \cdot \rho_{H_2} \cdot K \cdot L_{heat}^2} \ll 1,$$

where L_{gas} and L_{heat} are the gas and heat diffusion paths, respectively. K, μ, and M are the powder permeability, and hydrogen viscosity and molecular weight. In our case, $N < 1 \times 10^{-8}$. Therefore, we disregard the effect of pressure gradient inside the canister.

The MH expansion during cycling (≈20% for $LaNi_5$) and the MH pulverization (and, thus, the porosity heterogeneity) are disregarded [42].

2.2.1. MH modeling

We evaluate the energy conservation equation as follows [43]:

$$(\rho c_p)_e \frac{\partial T}{\partial t} = k_e \nabla^2 T + \dot{q}, \tag{1}$$

where k_e is the effective thermal conductivity of the MH, $(\rho c_p)_e$ is the effective heat capacity of the MH, and $\dot{q}$ is the volumetric reaction heat source inside the MH. In turn, k_e and $(\rho c_p)_e$ read:

$$k_e = \xi k_{H_2} + (1-\xi) k_m, \tag{2a}$$

$$(\rho c_p)_e = \xi \rho_{H_2} c_{pH_2} + (1-\xi) \rho_m c_{pm}, \tag{2b}$$

The hydride thermal conductivity, density, and specific heat of the MH are k_{MH} = 2 W/m K, ρ_{MH} = 7260 kg/m^3, c_{pMH} = 419 J/kg K. f_{H_2} is the hydrogen mass flow rate, which is positive during charge, and negative during discharge.

In absorption, the reaction rate r is:

$$r = C_a e^{-\frac{E_a}{RT}} \ln \frac{p}{p_{eq}} \left(1 - \frac{m_{MH}}{m_t}\right), \tag{3}$$

while in desorption:

$$r = C_d e^{-\frac{E_d}{RT}} \frac{p - p_{eq}}{p_{eq}} \left(\frac{m_{MH}}{m_t}\right), \tag{4}$$

Finally, p_{eq} is calculated as follows:

$$p_{eq} = p_0 e^{\left[\frac{\Delta H}{RT} - \frac{\Delta S}{R} + \beta\left(\frac{m_{MH}}{m_t} - \frac{1}{2}\right)\right]}, \tag{5}$$

where $p_0 = 1$ bar is the reference pressure, ΔH and ΔS are the enthalpy, entropy variations respectively.

The heat source is:

$$\dot{q} = -\Delta H r (\xi \rho_{MH}) \frac{S_c}{M_{MH}}. \tag{6}$$

2.2.2. PCM modeling

The PCM melting and solidification is modeled through the enthalpy method (see for instance [44]):

$$\rho_{PCM} \frac{\partial H}{\partial t} = k_{PCM} \nabla^2 T \tag{7}$$

where H is the enthalpy and the relationship between H and the temperature inside the PCM is:

$$T = \begin{cases} H / c_{p,PCM}, & H \le c_p T_m \\ T_m, & c_p T_m < H \le c_p T_m + \lambda \\ (H - \lambda)/c_p, & H > c_p T_m + \lambda \end{cases} \tag{8}$$

The minimum mass of PCM m_{PCM} required to guarantee the absorption of the uptake heat is based on the reaction enthalpy, i.e.:

$$m_{PCM} = \frac{\%wt \cdot m_t \cdot \frac{\Delta H}{M_{H_2}}}{\lambda}. \tag{9}$$

2.3. Numerical solution and model validation

The numerical solution is obtained with the commercial package AnSys Fluent 2022 R2 [45]. UDFs were employed to instruct Fluent to solve the mathematical model hereby described for the hydrogen uptake and release. In particular, the UDFs cater for the solution of Eqs. (3) and (4) at each timestep. Eqs. (1), and (3) to (8) are discretized through a finite-volume approach that uses the least square-based method to approximate the gradients and the first order Euler implicit scheme for temporal integration. MH and PCM domains are explicitly coupled through the coupled wall boundary condition [45]. We comment that nor pressure–velocity coupling nor convective term discretization is necessary because p and velocity are constant in the whole domain. A fixed timestep of 0.5 s was selected for each simulation.

Boundary and initial conditions. At the MH-PCM interface, a switch in thermal conductivity is present, while the heat exchange mechanism remains conduction. Therefore, a two-side coupled wall boundary condition is applied at such interface.

Symmetry is applied both at the external surface (thermal insulation) and the axis of the canister:

$$\frac{\partial T_{b=b_2}}{\partial b} = \frac{\partial T_{b=b_0}}{\partial b} = 0 \tag{10}$$

This is also true in the longitudinal direction:

$$\frac{\partial T_{z=0}}{\partial z} = \frac{\partial T_{z=\mathcal{L}}}{\partial z} = 0 \tag{11}$$

Table 1
Parameters used for the calculations.

Parameter	Value	
C_a	59.2	s^{-1}
C_d	9.6	s^{-1}
ΔH_a	−30,478	J mol^{-1}
ΔH_d	30,800	J mol^{-1}
ΔS_a	−108	J mol^{-1} K^{-1}
ΔS_d	108	J mol^{-1} K^{-1}
E_a	21,170	J mol^{-1}
E_d	16,420	J mol^{-1}
p_0	1	bar
β	0.13	–
S_c	3	–

When fins are present in the system, a two-side coupled wall is also applied at the interface between the MH and the fins, and between the PCM and the fins, since the thermal conductivity value changes from one domain to another. The initial conditions are expressed as follows:

Absorption phase	Desorption phase
$T_{MH} = T_{PCM} = T_m$	$T_{MH} = T_{PCM} = T_m$
$p = p^a_{H_2} = 30$ bar	$p = p^d_{H_2} = 1$ bar
$\frac{m_{MH}}{m_t} = 0$	$\frac{m_{MH}}{m_t} = 1$

For cases A and B, only a portion of the total canister is selected as domain. Specifically, case A is modeled as a 2D geometry, benefiting from the total axi-symmetry. Conversely, in case B the domain always comprises only one fin, benefiting from the periodic symmetry. Finally, case C is modeled as a complete 3D geometry, with no symmetry sections or domain reduction paths.

3. Model validation

Our solutions are validated and compared with data in the literature. We compare the results of our model in absorption and desorption with data from Laurencelle et al. [46]. Namely, two experiments were used as reference. The first experiment, named "small reactor", contains 1 g of $LaNi_5$, is charged at 6 bar and discharged at 0.068 bar. The external surface of such reactor is kept constant in an oven. The second experiment, named "large reactor", contains 25 g of $LaNi_5$, is charged at 12.7 bar and discharged at 0.086 bar, and the external surface exchanges convective heat with circulating water. The evolution of the storage capacity and the reactor temperature are shown in Figs. 2 and 3, respectively. Our numerical results present a good match with the experimental data.

For this and the following results, the parameters in Table 1 have been used [43].

3.1. Mesh sensitivity

Figs. 4 and 5 report the results of the mesh sensitivity analysis. This was conducted on the charge phase of 3D finned geometry (case B) with fin width 2 mm and fins number 16. The analysis accounts for the absorption of 95% of the theoretical storage capacity. Four mesh sizes were considered. In the following, the case with 33k cells is chosen as appropriate to continue our study. In fact, no appreciable difference is present when further increasing the size from 33k cells to 60k cells.

3.2. Impact of natural convection in the PCM

The impact of Natural Convection (NC) in the PCM has been assessed in order to ascertain whether it can be disregarded, allowing for more efficient simulations. The comparison was made on the absorption phase for case A (base cylinder geometry), activating/deactivating the flow equation in the PCM domain. Fig. 6 shows that no appreciable difference is present between the results obtained with NC and without NC as for the storage capacity curve (state of charge of the canister). The temperature profile is in good agreement as well. These results are also in accordance with the simulations of Tao et al. [47], who drew the same conclusions for a horizontally-oriented PCM canister surrounding an inner tube where a High Temperature Fluid flows, thus exchanging convective heat. They also prove that NC does not significantly affect the heat storage capacity of the PCM. Therefore, all results in the present work are obtained without NC in the PCM.

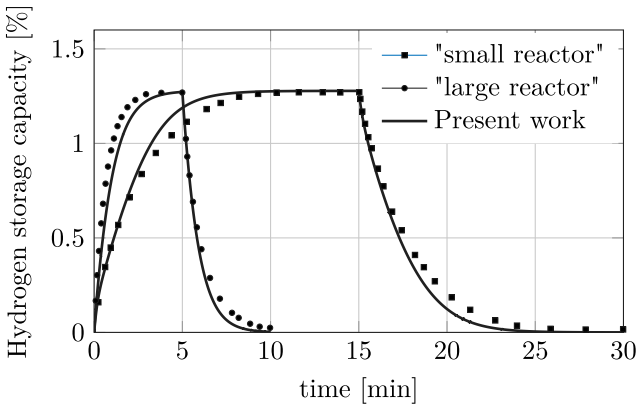


Fig. 2. Validation of the absorption and desorption profiles. Experimental data from [46].

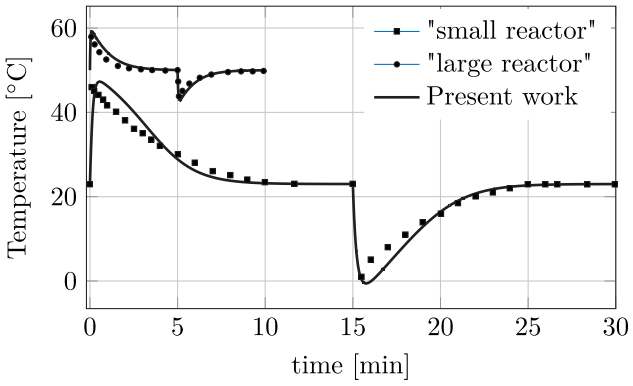


Fig. 3. Validation of the temperature profiles. Data from [46].

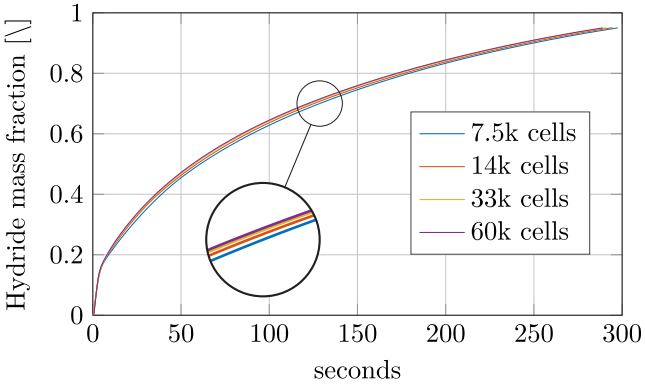


Fig. 4. Mesh sensitivity analysis. Results of the absorption profiles.

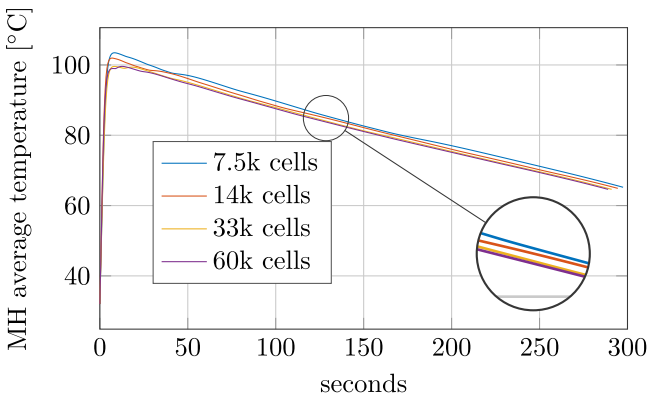


Fig. 5. Mesh sensitivity analysis. Results of the temperature profiles.

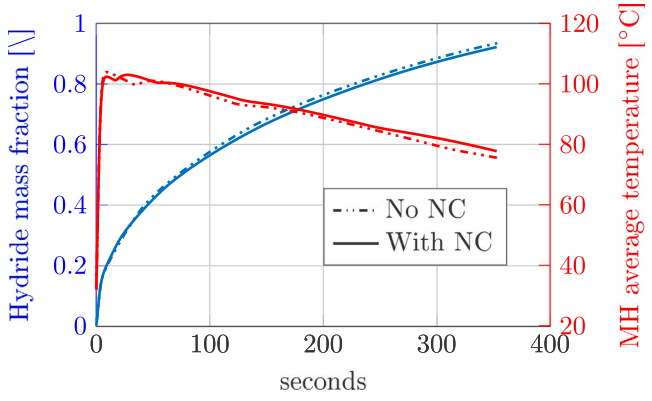


Fig. 6. Hydride mass fraction and MH temperature during absorption in case A. Results with and without NC.

3.3. Impact of model discretization

For relatively simple geometries like case A, 1D models can also be applied, instead of more complicated and resource-consuming 2D or 3D discretizations. In order to ascertain whether the assumption of no axial nor circumferential variability of temperature and reaction rate is valid, we compared results obtained with 1D and 2D models as a function of the canister aspect ratio when a fixed-temperature boundary condition is applied at the bottom of the vessel. Figs. 7 and 8 show that the difference between the results obtained with the 1D model and the 2D model is not significant for $\mathcal{L}/d > 5$, i.e., long and thin canisters, being Fo= $\frac{t \cdot \alpha_{MH}}{\mathcal{L}^2}$ the Fourier number. Conversely, thick and short vessels present a more relevant discrepancy between the two discretization models. The Relative Root Mean Square Error is also represented as a function of $\mathcal{L}/d$.

However, it is noteworthy that the reaction time is not a function of the model discretization. In fact, both in absorption and desorption, the profiles for 1D and 2D tend to converge towards the end of the reaction. This demonstrates that relatively simple and straightforward 1D models can be applied whenever the temporal temperature distribution within the vessel is not important, but only the ab/desorption time. These results are in agreement with those of [30] (cfr. Section 1).

4. Results and discussion

Fig. 9 shows that the absorption time to reach 95% of the storage capacity in case A is t_a =374 s. The estimated average equivalent absorption power $\overline{P} = \frac{1\ \text{kWh}}{t_a}$ is 9.62 kW. The temperature is slightly above 100 °C for a brief initial phase and then linearly reduces with time. At the end of absorption, the temperature is still significantly

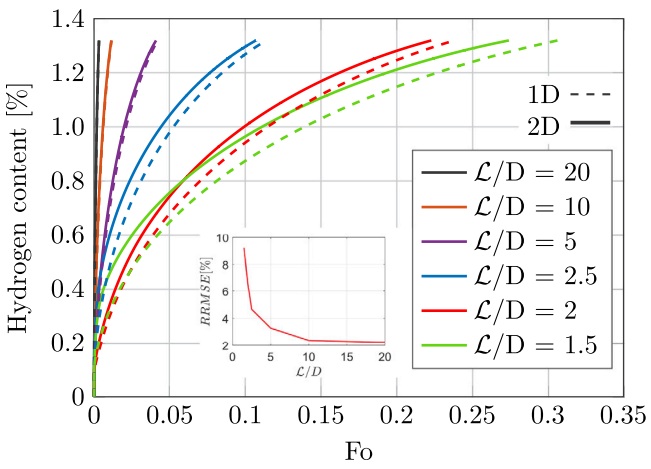


Fig. 7. Hydrogen storage capacity as a function of the model discretization (1D/2D) and aspect ratio in absorption.

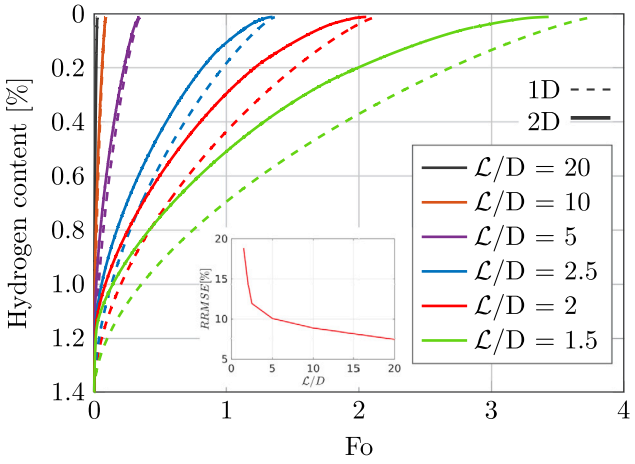


Fig. 8. Hydrogen storage capacity as a function of the model discretization (1D/2D) and aspect ratio in desorption.

higher (≈80 °C) than the initial value (30 °C). Desorption is slower than absorption, taking up to 1845 s to release 95% of the initially stored hydrogen (Fig. 10). The average equivalent desorption power is therefore 1.95 kW. This can be explained considering the lower kinetic constant C in desorption than in absorption and that the pressure term in Eq. (4) is lower than in (3), due to hydrogen being discharged at 1 bar and charged at 20 bar.

Case B (base cylinder with 16 fins of 2 mm width) is 20.7% faster in absorption and 24.1% faster in desorption than case A, requiring 243 s and 1199 s to absorb and desorb 90% of the total amount of hydrogen, respectively. Case A requires 316 and 1581 s to absorb and desorb the same amount of hydrogen. Consistently, the average reactor temperature is lower (in absorption) and higher (in desorption) in case B than in case A, demonstrating a more efficient heat exchange between the MH and the PCM. Such an increase in efficiency is due to the increased heat exchange surface area between the two materials, thanks to the presence of 16 fins inside the PCM domain.

Finally, we focus on a novel geometry whereby the MH powder is contained in a helix-shaped tube immersed in the PCM (case C). The geometry of the helix has been selected in order to maintain the same amount of stored hydrogen. In other words, the internal volume of the helix is the same as that of the inner cylinder in cases A and B. In turn, case C is divided into 2 further sub-cases, namely C.1 and C.2. C.1 has h_p = 70 mm, h_d = 14.81, mm, and h_D = 50 mm, and the same

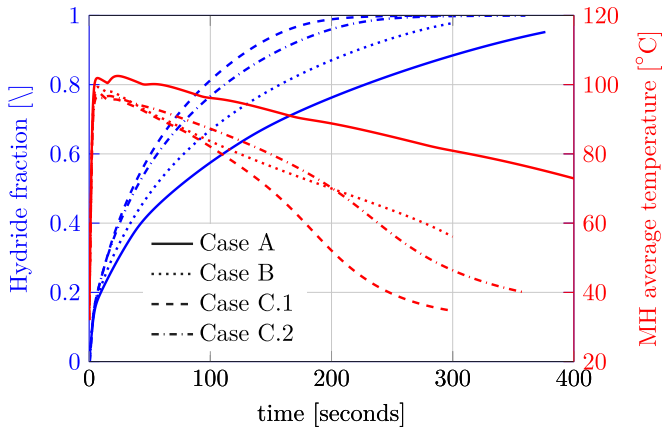


Fig. 9. Hydride fraction and temperature profiles for cases A, B and C in absorption.

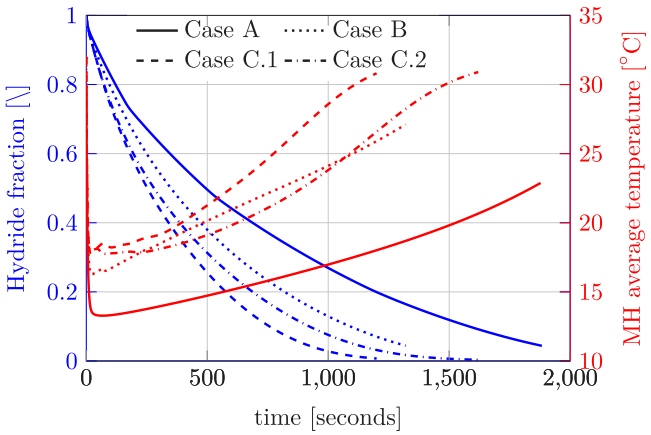


Fig. 10. Hydride fraction and temperature profiles for cases A, B and C in desorption.

external radius and length of the canister (and, thus, total volume) as those of cases A and B, to make a comparison with equal volumetric density. This layout does not uses the PCM in a reasonable manner. In fact, much of the PCM does not intervene in the process and does not exchange heat. C.1 has approximately 6 times the amount of the PCM needed for the operation (≈4400 cm^3 vs. 755.2 cm^3). Therefore, we improved such layout to C.2, where radius and pitch of the helix, as well as the radius and length of the canister have been adjusted to better optimize the PCM mass. In this configuration, h_p = 28 mm, h_d = 16 mm, h_D = 50 mm, $\mathcal{L}$ = 530 mm, and b_2 = 35 mm. The volume of PCM is 1370 cm^3.

Figs. 9 and 10 report the ab/desorption curves for case C as well. The figure shows that C.2 is slightly slower in ab/desorbing the same amount of hydrogen than C.1, whereas it increases the volume and mass density of the storage system. We believe that the slight reduction in storage efficiency is justified by a better usage of the PCM and is therefore acceptable. The absorption and desorption processes are considerably faster in cases C.1 and C.2 than in Case A. In absorption, we note a reaction time reduction of −57.8% and −48.9% for case C.1 and C.2, respectively. In desorption, the reduction is −51.2% for case C.1 and −40.3% for case C.2. The great advantage of using the helix-shaped system lies in the augmented heat exchange surface between the MH and PCM and from the considerably lower heat diffusion path. Such heat diffusion path is equal to the helix radius, namely 7.4 mm and 8 mm in cases C.1 and C.2, respectively, whereas it is equal to 10.2 mm in case A and B.

Designs C.1 and C.2 are also faster than the finned geometry, although the advantage is less evident. Similarly to case A, case B is slower to ab/desorb hydrogen due to the higher heat diffusion path compared to C.1 and C.2. This factor implies that the heat developed at the center of the MH tube, being it positive or negative (i.e., in absorption or desorption, respectively) is farther away from the nearest PCM node than it is in case C.1 or C.2. At the same time, in spite of the presence of many fins, the heat exchange surface area is greater in the helix tube than it is in case B. Due to the higher energy density of the helix shape compared to the finned geometry, the former performs better in both stationary and mobile applications.

Case C.1 and C.2 exhibit a 0.26% and 0.62% gravimetric density. The latter value is the higher achieved in this work among all the investigated layouts, thus demonstrating that case C.2 is superior to case B both in terms of charge/discharge power and energy density.

Figs. 9 and 10 also show that the average temperature in the reactor is much lower/higher in case C.1 than in case A throughout the whole absorption/desorption process. Accordingly, the temperature profile of C.2 lies in between cases C.1 and A.

Fig. 11 shows that the average absorption power is significantly higher than the desorption one, for all the cases. Furthermore, case C.1 presents the highest average power in both absorption and desorption among the investigated cases. Case C.2, conversely, has a slightly lower average power but a significantly higher energy density, both gravimetric and volumetric. Cases A, B, and C.1 share the same volumetric density, having the same geometrical parameters (radius and length). Nonetheless, adding 16 Aluminum fins to the bare cylindrical design reduces the gravimetric density to the lower value between the 4 configurations, i.e., 0.24%, while increasing the ab/desorption rate. In other words, the increased heat exchange surface area between the MH and the PCM, thanks to the fins, is accompanied by a relevant increase in weight, albeit not in volume. The strength of the novel design C.2 resides in its capacity to increase both energy density and reaction rate.

Figs. 12 and 13 show the temperature and liquid fraction distributions for case C.2 at t = 60 s (hydrogen content = 60%) and 200 s (hydrogen content = 95%) in absorption, and t = 60 s (hydrogen content = 80%) and 1000 s (hydrogen content = 8%) in desorption, respectively. The temperature is relevantly higher/lower in correspondence to the helix center than at the MH-PCM interface during the ab/desorption. It is also apparent how the PCM melts and solidifies faster in the vicinity of the helix, while struggling to change phase at the center of the canister (in the vicinity of the longitudinal symmetry axis). The temperature-liquid fraction distribution suggests to decrease h_D, i.e., reduce the spiral outer diameter, and employ longer canisters, while preserving the same total volume. This should reduce the statistical mean distance between a random point in the PCM domain and the closest MH-PCM interface.

4.1. Impact of fins thickness

In case B (base cylinder with longitudinal fins), the fins thickness has been varied between 1 mm and 4 mm. The step is 0.5 mm, except between 3 mm and 4 mm, where it is 1 mm. Therefore, we analyze 6 sub-cases in total (Table 2). The number of fins is 16 for each sub-case, equally spaced.

Figs. 14 and 15 summarize the results of the sensitivity analysis in absorption and desorption, respectively. In both phases, an increase in fin thickness leads to a reduction in the reaction time. This is clearly explained by considering the augmented heat exchange surface between the MH and the PCM, thus facilitating the heat transfer from/to the MH in ab/desorption, respectively. The impact on the reaction time is slightly non-linear but it is nearly equal between absorption and desorption, with a maximum reduction of −32.88% in absorption and −33.34% in desorption when adding 16 fins with thickness 4 mm to the base cylinder of case A. The benefit of adding fins to the canister is decreasing as the fin thickness increases.

Despite the positive impact of the fin thickness on the charge/discharge time, an increase in fin thickness leads to an increase in

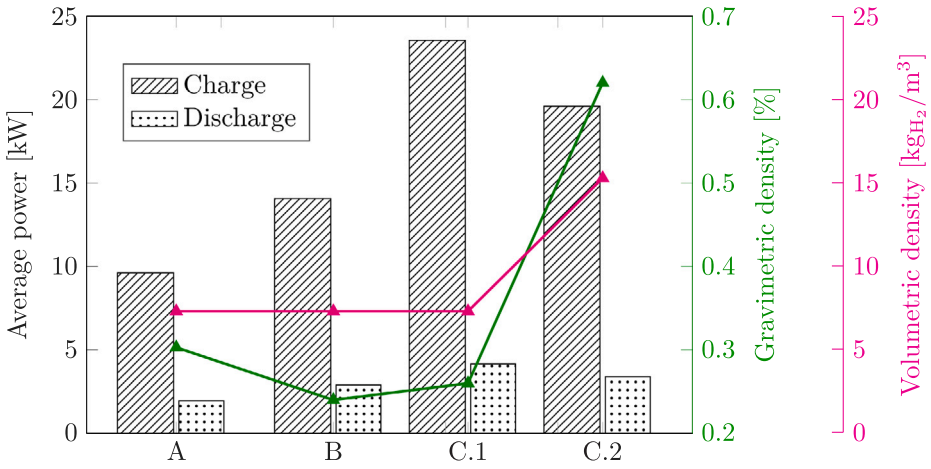


Fig. 11. Average ab/desorption power and energy density for all the four cases.

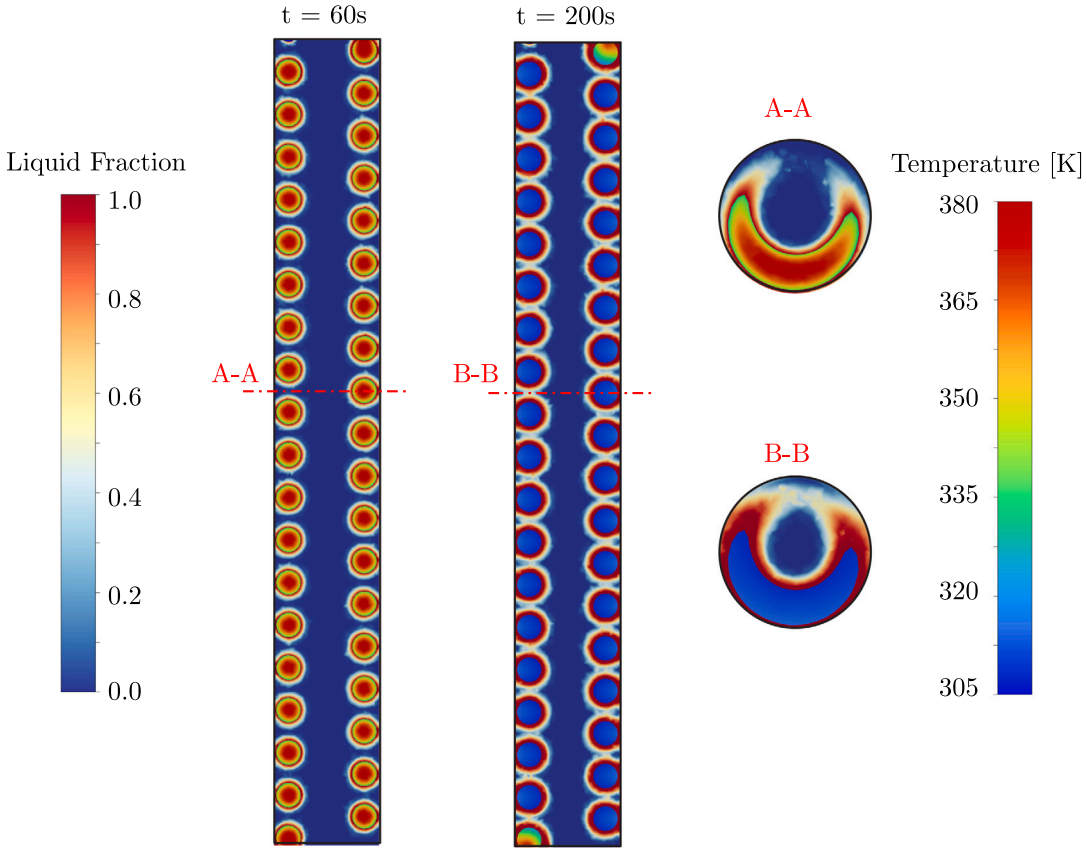


Fig. 12. Temperature in the MH and liquid fraction in the PCM for case C.2 in absorption at t = 60, and 200 s.

Table 2
Summary of sensitivity analysis of case B.

Case	Sensitivity to fin thickness						Sensitivity to number of fins				
	B.1	B.2	B.3	B.4	B.5	B.6	B.7	B.8	B.9	B.10	B.11
Fin thickness [mm]	1	1.5	2	2.5	3	4	1	2	2	2	3
Number of fins	16	16	16	16	16	16	8	8	12	20	20

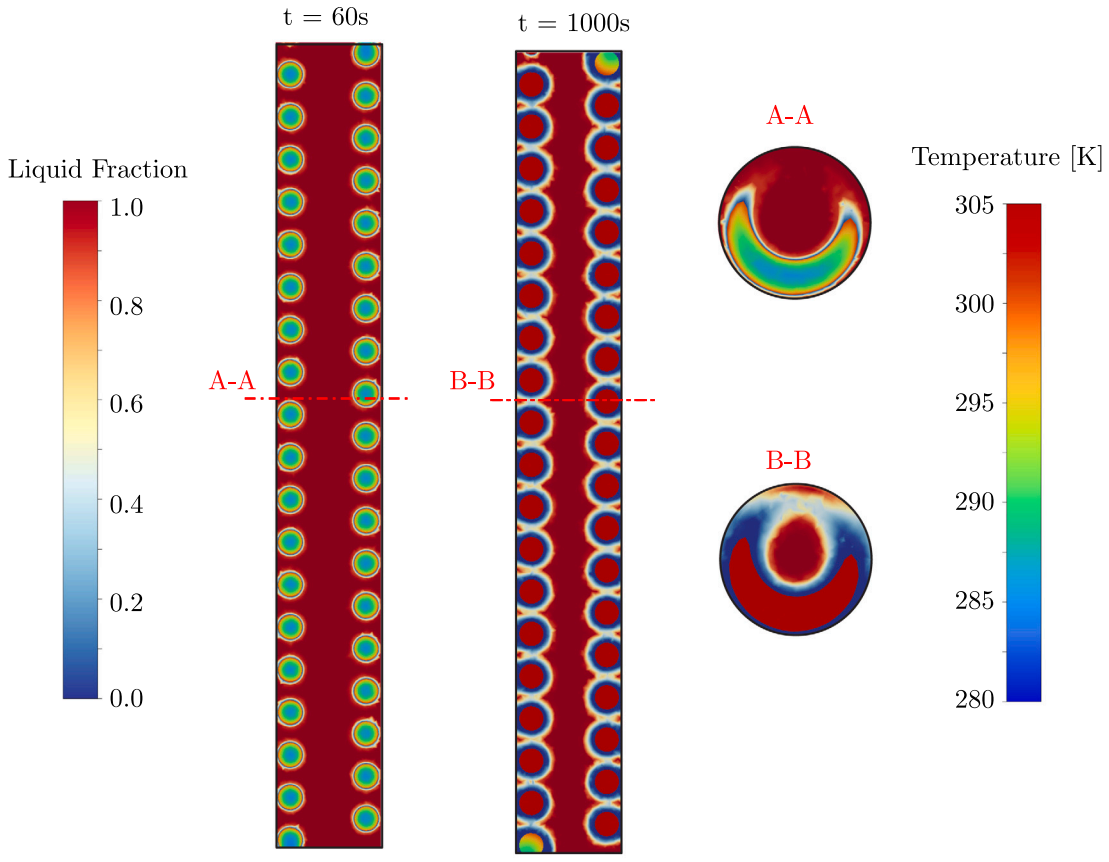


Fig. 13. Temperature in the MH and liquid fraction in the PCM for case C.2 in desorption at t = 60, and 1000 s.

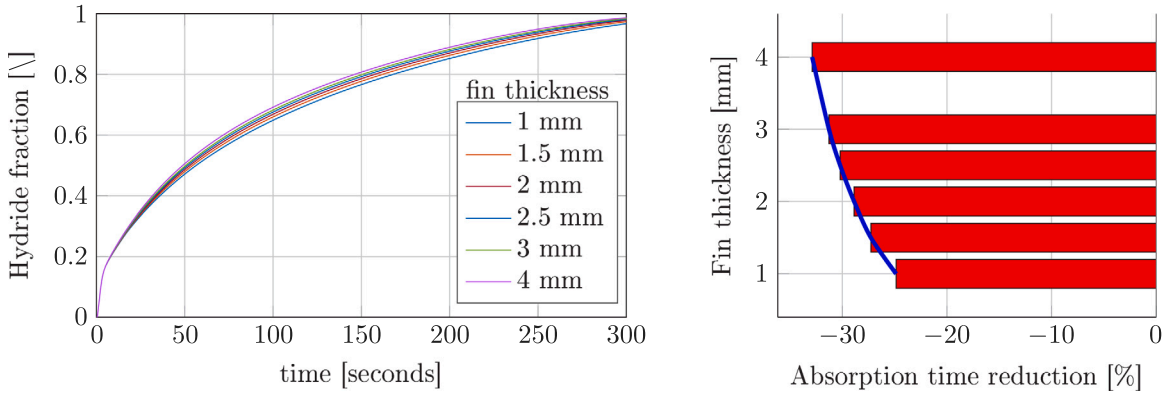


Fig. 14. Sensitivity analysis to fin thickness in absorption. **(left)** Absorption curve and **(right)** absorption time compared to case A.

the total mass of the system as well. This can significantly impair the gravimetric density of the system. To address such issue, Fig. 16 shows the impact of the fin thickness on the system energy density and weight. We note that the global gravimetric density of the system (hydrogen stored per unit mass of the canister) reduces from 0.30% to 0.20% when increasing the fin width from 0 mm (no fins) to 4 mm, while the total weight increases from 10.3 kg to 14.71 kg. This means a shift from 0.10 kWh/kg to 0.068 kWh/kg. The weight of the PCM slightly reduces due to the decreased available space, occupied by the fins, but the positive difference in density of the two materials ($\rho_{\text{fin}} - \rho_{\text{PCM}} > 0$) leads to a globally negative impact on the energy density of the storage system.

The analysis so far presented does not allow to find an optimal solution to the investigated problem. In fact, the increase in fin width almost linearly improves the heat exchange while decreasing the energy density. In order to deepen the analysis, a second sensitivity study is conducted on the fin number.

4.2. Impact of fins number

The number of fins has been varied between 8 and 20, at steps of 4. The fin thickness is the same for each simulation, namely 2 mm. In addition, we analyze two more cases: a configuration with the minimum number of fins with the smallest thickness (8 fins with 1 mm width), and the maximum number of fins (20) with 3 mm fins. These two additional cases helps us understand whether trend patterns differ in the considered range of the sensitivity analysis. Therefore, we have 6 sub-cases total (Table 2). Note that the case with 16 fins of 2 mm width has been already investigated in the sensitivity analysis to the fin thickness. Since the number of fins in sub Section 4.1 is 16, this

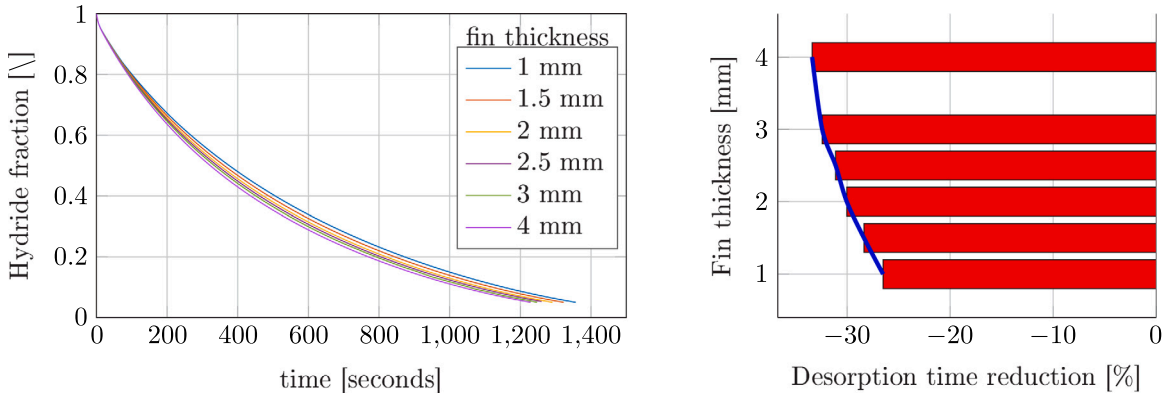


Fig. 15. Sensitivity analysis to fin thickness in desorption. **(left)** Desorption curve and **(right)** desorption time compared to case A.

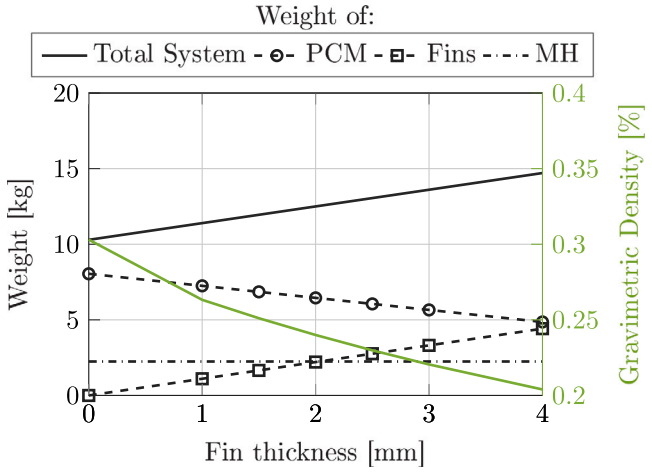


Fig. 16. Weight and gravimetric density as a function of fin thickness (case B).

number is taken as baseline in the following study. Note that such a baseline configuration (16 fins with 2 mm width) is already 28.9% faster in absorption (266 s vs. 374 s for 95% absorption) and 30.0% faster in desorption (1291 s vs. 1845 s to desorb 95%) than case A. Figs. 17 and 18 show the summary of the sensitivity analysis to the fins number for the absorption and desorption phases, respectively. A nearly linear trend is visible for the ab/desorption time variation. With a 2 mm fin width, by increasing the number of fins from 16 to 20 there is a −3% reduction in reaction time, both in absorption and desorption. Conversely, by decreasing the number from 16 to 8, the reaction times increase by 10%. The two end cases, marked with ∗ and † and using 1 mm and 3 mm fin width, respectively, show that the trend is preserved throughout the considered range.

As well as for the sensitivity study to the fin thickness (cfr. sub Section 4.1), the fins number does not allow to infer a guideline on the optimization of a finned canister. In fact, the higher the number of fins, the greater the storage performance in terms of charge/discharge time. This has the same reason as of the reduction in reaction time when increasing the fins width. When we install more fins on the external surface of the MH inner tube, we extend the heat exchange surface between the MH and PCM, thus fostering the reaction. However, similarly to what we pointed out in Sub Section 4.1, we also reduce the energy density by increasing the number of fins. This can be visually appreciated in Fig. 19, which shows the impact of the fins number on the system energy density and on the total weight of the system. The global gravimetric density decreases from 0.283% (or 0.094 kWh/kg) to 0.271% (0.090 kWh/kg) when increasing the fins number from 8 to 20 and maintaining the fins width to 2 mm. This translates in an increase of the total weight from 10.6 kg to 11.06 kg.

The comparison of Fig. 19 with Fig. 16 allows to infer a general rule about the optimization of finned MH-PCM configurations. It is generally preferable to use a greater number of thin fins instead of few thick fins. In fact, for the same fins weight, thin fins allow for a greater heat exchange surface. For instance, 16 fins of 1 mm or 8 fins of 2 mm occupy the same volume and have the same mass, but the former option is much more efficient (−18.3% against −11.1% with respect to case A). Vice versa, 16 fins of 1 mm and 12 fins of 2 mm have approximately the same impact on the absorption time (≈ − 18.5% compared to case A) but the latter option is heavier (12.7 kg against 14 kg).

Figs. 20 and 21 show the distribution of the temperature inside the MH and the PCM liquid fraction for different fins number in absorption and desorption. The fields are represented at$t$ = 30 s (hydride fraction ≈35%) and$t$ = 210 s (hydride fraction ≈85%) for absorption and at$t$ = 30 s (hydride fraction ≈90%) and t = 1000 s (hydride fraction ≈15%) for desorption. During absorption, the temperature inside the MH is lower in the vicinity of the MH-PCM interface, due to the convective heat exchange with the PCM. Vice versa, the temperature is higher in proximity of the central artery, where the heat transfer is more problematic due to the relatively great distance from the heat sink. The opposite is true for the desorption phase, where the MH is at a lower temperature than the PCM and the temperature gradient is negative moving from the MH-PCM interface towards the central canister artery. Furthermore, it can be seen that the fins, irrespective of their number and dimensions, do not present any temperature gradient, i.e., the temperature is homogeneous inside the fin at all times. This is due to the significantly higher thermal conductivity of Al when compared to the MH and the PCM, thus the heat transfer is relatively fast inside the fin. Finally, we comment that the fins help to transfer heat to/from the MH as the PCM melts and solidifies in the vicinity of the fin as well as in the vicinity of the MH.

4.3. Effect of fin material

We subsequently conducted a sensitivity analysis to the fins material, comparing results obtained with aluminum, copper, and steel. Fig. 22 shows the results for the absorption phase. Namely, copper and aluminum do not present any significant differences in terms of charge power, while steel shows a slightly lower performance. The density of steel and copper is around 3 times higher than aluminum, making them unsuitable as a fin material. In fact, employing steel or copper would significantly increase the weight of the system and the materials cost without affecting the storage efficiency (copper) or even negatively affecting it (steel). For instance, case B would weight 17.60 kg instead of 12.50 kg (+ 41%) if copper fins are employed in place of aluminum ones.

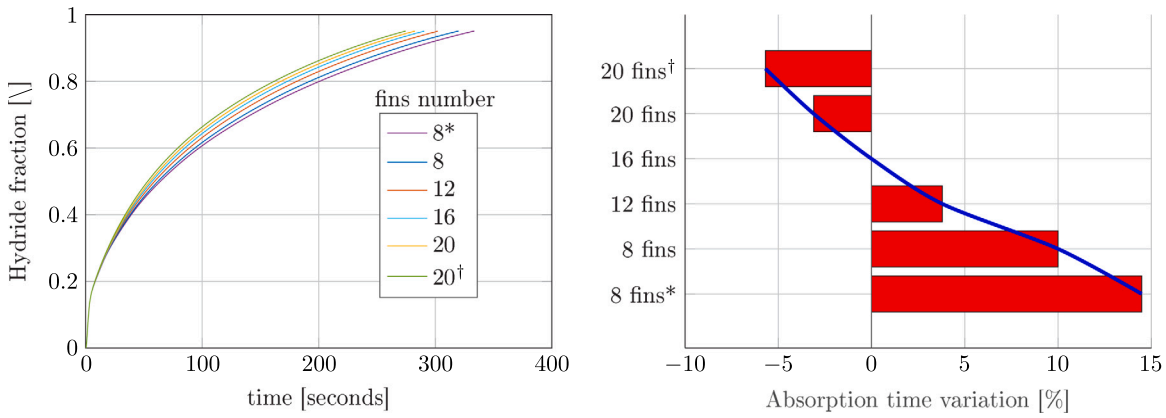


Fig. 17. Sensitivity analysis to fin number in absorption. **(left)** Absorption curve and **(right)** absorption time comparison. * 1 mm width; † 4 mm width.

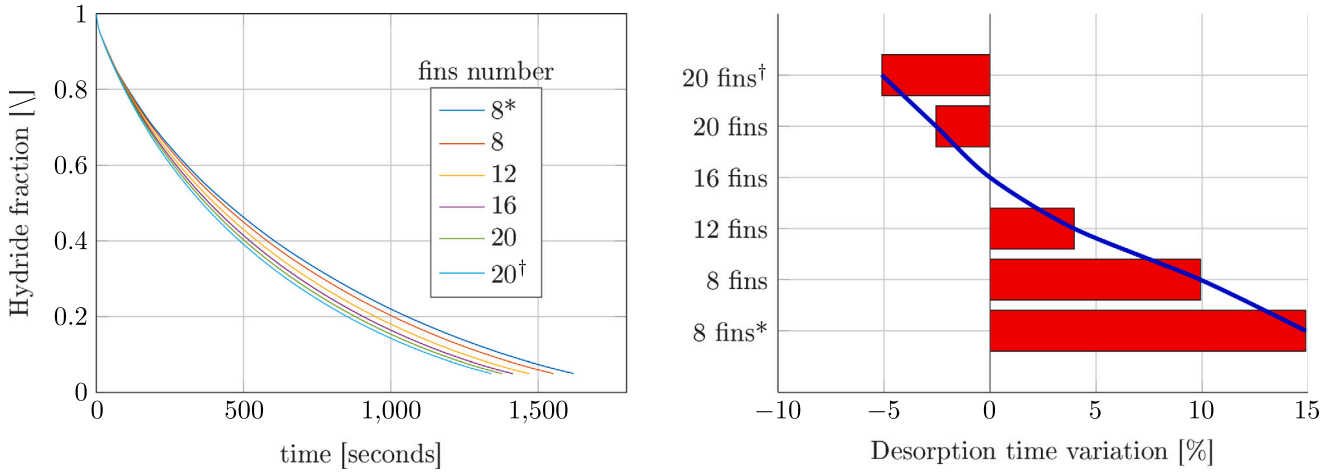


Fig. 18. Sensitivity analysis to fin number (case B) in desorption. **(left)** Desorption curve and **(right)** desorption time comparison. * 1 mm width; † 4 mm width.

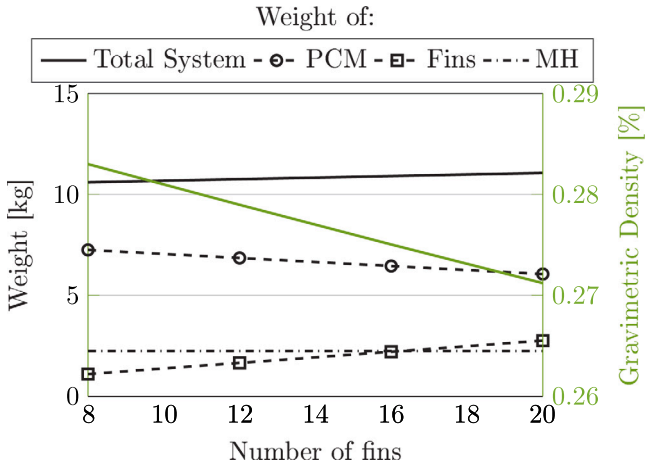


Fig. 19. Weight and gravimetric density analysis of the fin number sensitivity investigation.

4.4. Performance comparison with literature

We compared our findings with advanced MH-PCM designs from existing literature, which we name Reactor 1, 2, and 3. Reactor 1 [29] contains 0.353 kg of $LaNi_5$ (0.15 kWh of stored energy) and 0.325 kg of $LiNO_3$ - $3H_2O$. The authors present two sub-configurations of such reactor, which achieve 0.41% and 0.26% gravimetric density, respectively. The volumetric density is 14.76 and 11.82 kg_{H_2}/m^3, for the better design. The gravimetric and volumetric density is lower than our design C.2 (0.62% and 15.30 kg_{H_2}/m^3). As for the comparison on the mean saturated ab/desorption levels (or average ab/desorption power) we have: 0.536 kW and 0.342 kW, respectively, for Reactor 1. If we only account for 90% of saturation, the average absorption power is 1.53 kW. C.2, conversely, exhibits 19.6 kW and 3.4 kW as absorption and desorption average power, respectively.

Reactor 2 [48] contains 500 g of Mg (approximately 1 kWh of H_2) and reaches 90% of absorption level in 607 s (estimated average power 5.93 kW) with a gravimetric and volumetric density of 0.18% and 5.26 kg_{H_2}/m^3, respectively. Both absorption average power and storage efficiency are lower than case C.2. Especially the high number of fins (28) contributes to reduce drastically the gravimetric density of Reactor 2.

Finally, Reactor 3 [37] contains a series of Mg discs of 7.6 g and 44.4 g of $NaNO_3$ as PCM. The pile of discs exhibits 0.733% as gravimetric density, higher than case C.2. If a pile of 4 discs is considered, so that approximately 1 kWh of hydrogen is stored, the average absorption power is 3.40 kW while the average desorption power is 0.767 kW. This shows that a higher gravimetric density impairs the ab/desorption rate of this configuration. Overall, case C.2 compares relatively well with advanced configurations already presented in literature.

We comment that the finned canister (case B) is relatively easy to manufacture, being a straight tube with heat exchange longitudinal fins. An external container envelopes the surrounding PCM sectors, especially when in liquid form. The helix-shaped geometry (case C) is

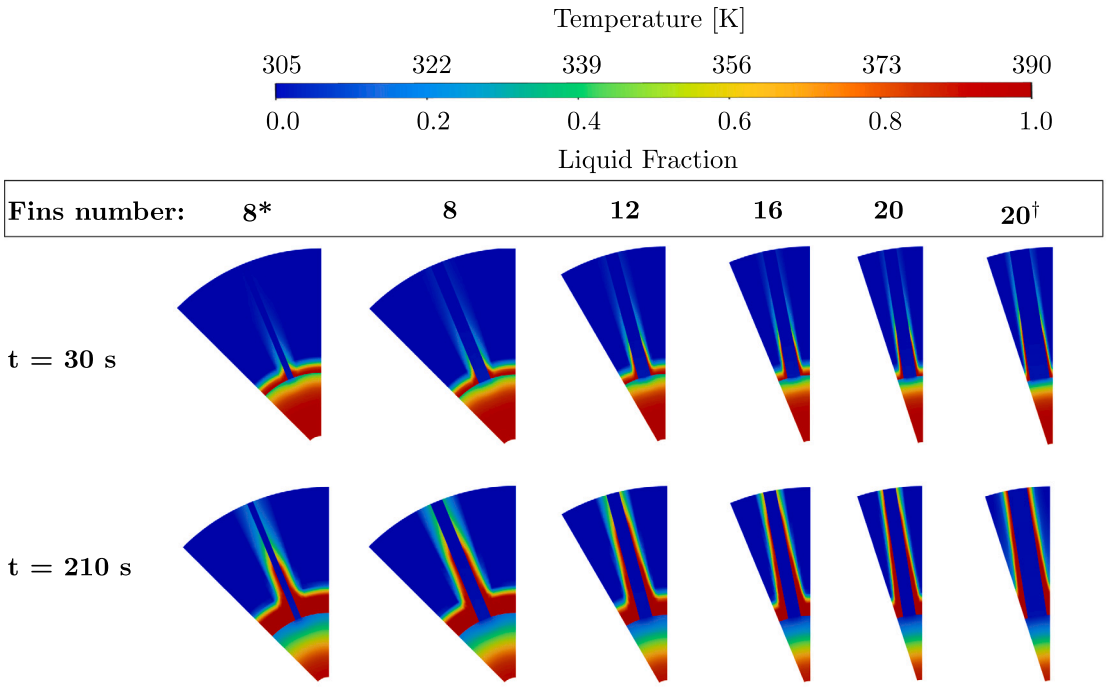


Fig. 20. MH temperature and PCM liquid fraction during absorption for different fins number and times.

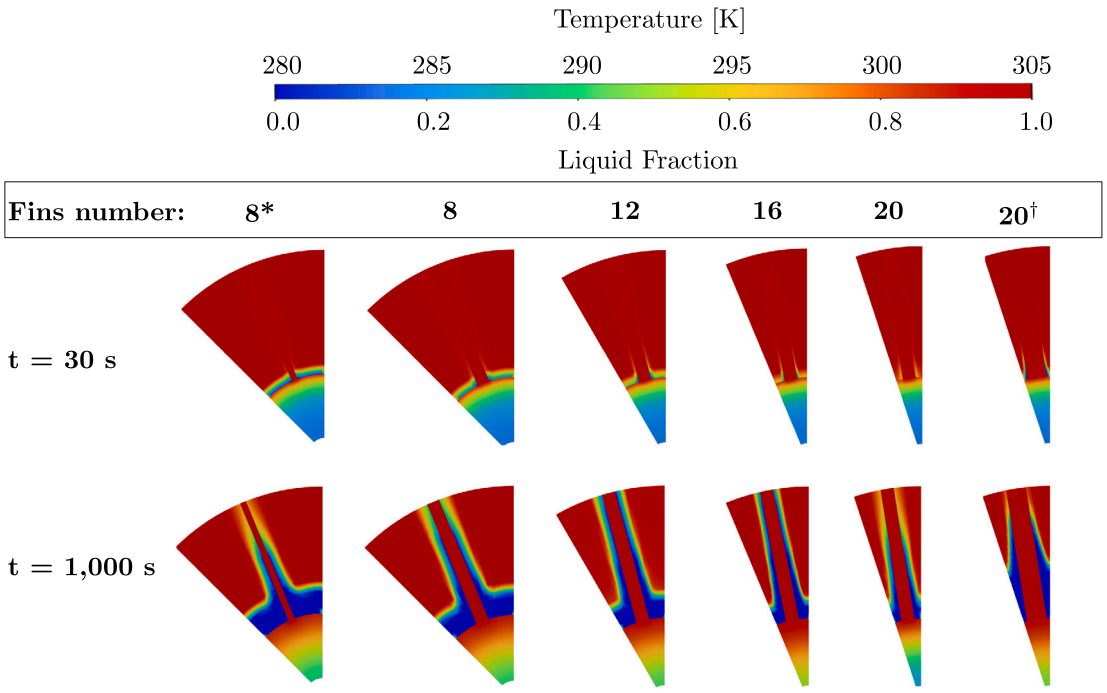


Fig. 21. MH temperature and PCM liquid fraction during desorption for different fins number and times.

comparatively more difficult to build, although pre-arranged helix heat exchange tube are already manufactured. The surrounding PCM can be easily poured in liquid form and then let solidified to completely envelope the helix tube.

The proposed designs are more suitable for small-scale applications. In fact, by scaling up the system, we expect the heat diffusion path to proportionally increase. As a consequence, the storage efficiency would be reduced. Furthermore, only a few studies have focused on big-scale applications and canisters, so that we have a limited knowledge on the effects on the storage system when scaled up. However, studying the possibility of modular applications is of interest: a series of the recommended design of the individual helix-shaped canister can be used to increase the delivered power, which is especially useful during the desorption stage. In order to reduce the impact on the volumetric density, which would unavoidably decrease, a number of helix canisters can be also inserted into the same container, where liquid PCM is poured to completely envelope all the tubes. The integration of such MH-PCM storage system into existing hydrogen storage infrastructures is subjected to considerations related to the storage pressure. In particular, our system was sized for small pressure ranges (e.g., 5 to 30 bar). However, this does not prejudice its possible usage for medium or even large pressure applications, especially in light of the relatively high

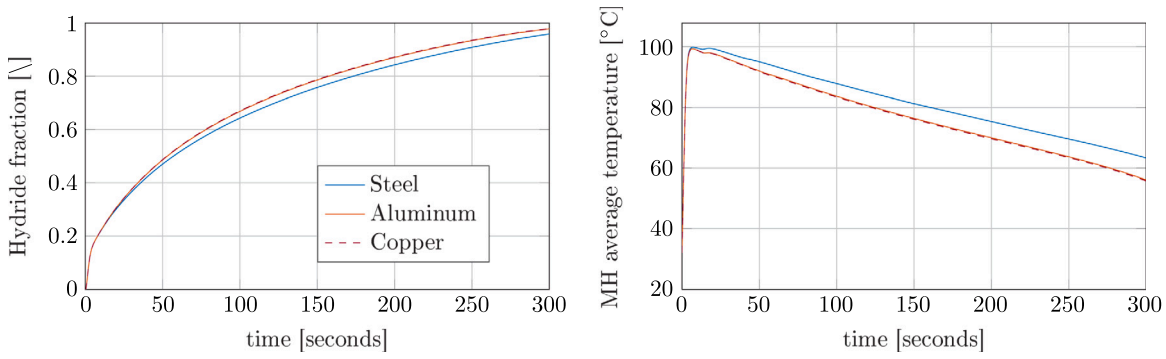


Fig. 22. Sensitivity analysis to the fin material for the absorption phase.

volumetric density exhibited by design C.2. The second consideration to be made is related to the specific dynamics and power density of our design. Hydrogen must be delivered quickly whenever short recharge time are needed. On the contrary, we comment that the desorption stage is the critical one of the charge/discharge cycle. This means that this design is preferable for applications where quick recharge time is not the fundamental factor (e.g., stationary application or in-board propulsion system for very small quadricycles).

5. Conclusions

Metal Hydrides can store hydrogen in solid form by means of chemical bonds with metals or metal alloys, thus providing a low pressure and safe hydrogen storage option. While addressing the heat management of such storage solutions, the coupling of the Metal Hydrides with a suitable Phase Change Material constitutes a passive way of controlling the Hydride temperature through melting and solidification.

Three Metal Hydride - Phase Change Material configurations were investigated and compared through a 3D mathematical model which accounts for the absorption and desorption kinetics of the reactions. Case A is a base cylinder design, case B is a finned cylinder geometry, and case C is a novel helix-shaped tube containing the hydride powder and immersed in Phase Change Material. Case B is further divided into 11 sub-cases to assess the impact of the fins thickness and number on the storage efficiency. $LaNi_5$ is selected as MH, whereas $LiNO_3$ - $3H_2O$ is selected as PCM.

Results can be summarized as follows:

- the ab/desorption of 1.04 kWh of hydrogen in case A (bare cylinder layout) can be achieved in less than 400 s and 1900 s, respectively. The estimated average ab/desorption powers are 9.62 kW and 1.95 kW. The gravimetric density achieved is 0.30%.
- fins help to reduce the reaction time in both absorption and desorption. By keeping the same weight, it is preferable to have a higher number of thin fins instead of a lower number of thicker fins. 16 fins of 2 mm reduce the cycle time of 29.5% with respect to case A. By increasing the fin thickness to 4 mm, the cycle time reduces by 33% but the gravimetric density goes down to 0.20%. By reducing the fin number from 16 to 8, the cycle time increases by 10.0%.
- the mass energy density of the storage system can be significantly impaired by the addition of fins. Therefore, it is imperative to find a trade-off between reducing cycle time and increasing total weight. The decision ultimately depends on the final applications of the storage system, be it mobile or stationary.
- the novel helix-shaped geometry (specifically, case C.2) reduces the ab/desorption time by 49% and 40% with respect to case A. This shows the worthiness of such new design, which also exhibits the higher gravimetric density (0.63%).
- the fin material affects the storage efficiency insomuch copper, aluminum, and steel exhibit very similar performances in terms of cycle time but aluminum is much lighter, thus resulting the best option for the longitudinal fins.

With regards to last point of the summary, it appears crucial, for future developments of this work, to optimize the geometrical factors of the helical design, i.e., inner tube radius, pitch, helix diameter. This is particular useful to better use the surrounding PCM and increase both gravimetric and volumetric density of the storage system. The numerical study hereby presented will then be followed by evaluations on the scalability of the storage systems, i.e., effect of the mass of hydrogen stored on the system efficiency. Finally, an executive project for the prototypes of the proposed designs, for experimental applications and studies, will follow.

CRediT authorship contribution statement

Marco Maggini: Writing – review & editing, Writing – original draft, Software, Methodology, Investigation, Data curation, Conceptualization. **Andrea L. Facci:** Writing – review & editing, Supervision, Resources, Project administration, Methodology, Investigation, Funding acquisition, Conceptualization. **Giacomo Falcucci:** Writing – review & editing, Supervision, Funding acquisition, Conceptualization. **Stefano Ubertini:** Writing – review & editing, Supervision, Resources, Funding acquisition.

Declaration of competing interest

The authors declare that they have no known competing financial interests or personal relationships that could have appeared to influence the work reported in this paper.

Acknowledgments

This project has been partially supported by the projects:

- PRIN P20223JMB3 - Modeling and optimization of sustainable hydrogen refueling infrastructures (HyREFI) and PRIN 2020BFX8JY - Hybrid Sustainable Mobility (HYSUM).
- ECS 0000024 Rome Technopole, CUP B83C22002820006, National Recovery and Resilience Plan (NRRP) Mission 4 Component 2 Investment 1.5, funded by the European Union-NextGenerationEU.
- National Recovery and Resilience Plan (NRRP), Mission 4 Component 2 Investment 1.3 - Call for tender No. 1561 of 11.10.2022 of Ministero dell'Università e della Ricerca (MUR); funded by the European Union – NextGenerationEU.

Data availability

Data will be made available on request.

References

[1] Li J, Fang J, Zeng Q, Chen Z. Optimal operation of the integrated electrical and heating systems to accommodate the intermittent renewable sources. Appl Energy 2016;167:244–54.

[2] Wu Y, Zhang T, Gao R, Wu C. Portfolio planning of renewable energy with energy storage technologies for different applications from electricity grid. Appl Energy 2021;287:116562.

[3] Mohler D, Sowder D. Energy storage and the need for flexibility on the grid. In: Renewable energy integration. Elsevier; 2017, p. 309–16.

[4] Rosati A, Facci AL, Ubertini S. Techno-economic analysis of battery electricity storage towards self-sufficient buildings. Energy Convers Manage 2022;256:115313.

[5] Koskela J, Rautiainen A, Järventausta P. Using electrical energy storage in residential buildings–Sizing of battery and photovoltaic panels based on electricity cost optimization. Appl Energy 2019;239:1175–89.

[6] Zhang F, Zhao P, Niu M, Maddy J. The survey of key technologies in hydrogen energy storage. Int J Hydrog Energy 2016;41(33):14535–52.

[7] Ubertini S, Facci AL, Andreassi L. Hybrid hydrogen and mechanical distributed energy storage. Energies 2017;10(12):2035.

[8] Facci AL, Sánchez D, Jannelli E, Ubertini S. Trigenerative micro compressed air energy storage: Concept and thermodynamic assessment. Appl Energy 2015;158:243–54.

[9] Facci AL, Cigolotti V, Jannelli E, Ubertini S. Technical and economic assessment of a SOFC-based energy system for combined cooling, heating and power. Appl Energy 2017;192:563–74.

[10] Facci AL, Ubertini S. Analysis of a fuel cell combined heat and power plant under realistic smart management scenarios. Appl Energy 2018;216:60–72.

[11] Loreti G, Facci AL, Baffo I, Ubertini S. Combined heat, cooling, and power systems based on half effect absorption chillers and polymer electrolyte membrane fuel cells. Appl Energy 2019;235:747–60.

[12] Abe JO, Popoola A, Ajenifuja E, Popoola O. Hydrogen energy, economy and storage: review and recommendation. Int J Hydrog Energy 2019;44(29):15072–86.

[13] Ye Y, Zhu H, Cheng H, Miao H, Ding J, Wang W. Performance optimization of metal hydride hydrogen storage reactors based on PCM thermal management. Appl Energy 2023;338:120923.

[14] Patil SD, Gopal MR. Analysis of a metal hydride reactor for hydrogen storage. Int J Hydrog Energy 2013;38(2):942–51.

[15] Niaz S, Manzoor T, Pandith AH. Hydrogen storage: Materials, methods and perspectives. Renew Sustain Energy Rev 2015;50:457–69.

[16] Bartolucci L, Krastev VK. On the thermal integration of metal hydrides with phase change materials: Numerical simulation developments towards advanced designs. SAE Technical Papers, 2022.

[17] Wang D, Wang Y, Wang F, Zheng S, Guan S, Zheng L, Wu L, Yang X, Lv M, Zhang Z. Optimal design of disc mini-channel metal hydride reactor with high hydrogen storage efficiency. Appl Energy 2022;308:118389.

[18] Sakintuna B, Lamari-Darkrim F, Hirscher M. Metal hydride materials for solid hydrogen storage: a review. Int J Hydrog Energy 2007;32(9):1121–40.

[19] Lundin CE, Sullivan RW. The safety characteristics of $LaNi_5$ hydrides. In: Hydrogen energy. New York, NY: Springer; 1975.

[20] Lewis SD, Chippar P. Analysis of heat and mass transfer during charging and discharging in a metal hydride-phase change material reactor. J Energy Storage 2021;33:102108.

[21] Facci AL, Lauricella M, Succi S, Villani V, Falcucci G. Optimized modeling and design of a PCM-enhanced H2 storage. Energies 2021;14(6):1554.

[22] Baykara SZ. Hydrogen: A brief overview on its sources, production and environmental impact. Int J Hydrog Energy 2018;43(23):10605–14.

[23] Krastev VK, Falcucci G. Comparison of enthalpy-porosity and lattice Boltzmann phase field techniques for the simulation of the heat transfer and melting processes in LHTES devices. In: E3S web of conferences 312. 2021.

[24] Mendecka B, Ilio GD, Krastev VK, Bella G. Technical assessment of phase change material thermal expansion for passive solar tracking in residential thermal energy storage applications. J Energy Storage 2022;48.

[25] Mendecka B, Ilio GD, Krastev VK, Bella G. Evaluating the potential of phase-change induced volumetric expansion in thermal energy storage media for passive solar tracking in high-temperature solar energy systems. Appl Therm Eng 2022;212.

[26] El Mghari H, Huot J, Tong L, Xiao J. Selection of phase change materials, metal foams and geometries for improving metal hydride performance. Int J Hydrog Energy 2020;45(29):14922–39.

[27] Marty P, de Rango P, Delhomme B, Garrier S. Various tools for optimizing large scale magnesium hydride storage. J Alloys Compd 2013;580:S324–8.

[28] da Cunha JP, Eames P. Thermal energy storage for low and medium temperature applications using phase change materials – A review. Appl Energy 2016;177:227–38.

[29] Dong X, Zhao H, Li H, Fucucci G, Zheng Q, Zhao H, Pu J. A novel design of a metal hydride reactor integrated with phase change material for H2 storage. Appl Energy 2024;367.

[30] Jemni A, Nasrallah SB. Study of two-dimensional heat and mass transfer during absorption in a metal-hydrogen reactor. Int J Hydrog Energy 1995;20.

[31] Yao J, Zhu P, Guo L, Duan L, Zhang Z, Kurko S, Wu Z. A continuous hydrogen absorption/desorption model for metal hydride reactor coupled with PCM as heat management and its application in the fuel cell power system. Int J Hydrog Energy 2020;45.

[32] Garrison SL, Hardy BJ, Gorbounov MB, Tamburello DA, Corgnale C, vanHassel BA, Mosher DA, Anton DL. Optimization of internal heat exchangers for hydrogen storage tanks utilizing metal hydrides. Int J Hydrog Energy 2012;37.

[33] Zhang S, Yang F, Zhou L, Zhang Y, Wu Z, Zhang Z, Wang Y. A novel multilayer fin structure for heat transfer enhancement in hydride-based hydrogen storage reactor. Int J Energy Res 2018;42.

[34] Nyamsi SN, Tolj I, Pasupathi S. Multi-objective optimization of a metal hydride reactor coupled with phase change materials for fast hydrogen sorption time. J Energy Storage 2023;71.

[35] Krastev VK, Bartolucci L, Bella G, Cordiner S, Falcucci G, Mulone V. Power vs. capacity performances of thermally integrated MH-PCM hydrogen storage solutions: current status and development perspectives. In: Proceedings of ECOS 2023. 2023, p. 2183–93. http://dx.doi.org/10.52202/069564-0197.

[36] Maggini M, Falcucci G, Rosati A, Ubertini S, Facci AL. Non-dimensional numerical analysis of coupled metal hydride - phase change material hydrogen storage system. J Energy Storage 2024.

[37] Ye Y, Ding J, Wang W, Yan J. The storage performance of metal hydride hydrogen storage tanks with reaction heat recovery by phase change materials. Appl Energy 2021;299:117255.

[38] Chaise A, de Rango P, Marty P, Frucharta D. Experimental and numerical study of a magnesium hydride tank. Int J Hydrog Energy 2010;35(12):6311–22.

[39] Bao Z, Yang F, Wu Z, Cao X, Zhang Z. Simulation studies on heat and mass transfer in high-temperature magnesium hydride. Appl Energy 2013;112:1181–9.

[40] Maad HB, Askri F, Nasrallah SB. Heat and mass transfer in a metal hydrogen reactor equipped with a phase-change heat-exchanger. Int J Therm Sci 2016;99:271–8.

[41] Mellouli S, Abhilash E, Askri F, Nasrallah SB. Integration of thermal energy storage unit in a metal hydride hydrogen storage tank. Appl Therm Eng 2016;102:1185–96.

[42] Nam J, Ko J, Ju H. Three-dimensional modeling and simulation of hydrogen absorption in metal hydride hydrogens torage vessels. Appl Energy 2012;89.

[43] Talaganis B, Meyer G, Aguirre P. Modeling and simulation of absorption–desorption cyclic processes for hydrogen storage-compression using metal hydrides. Int J Hydrog Energy 2011;36(21):13621–31.

[44] Voller V, Cross M. Accurate solutions of moving boundary problems using the enthalpy method. Int J Heat Mass Transfer 1981;24:545–56.

[45] Fluent user manual, https://www.afs.enea.it/project/neptunius/docs/fluent/html/ug/main_pre.htm.

[46] Laurencelle F, Goyette J. Simulation of heat transfer in a metal hydride reactor with aluminium foam. Int J Hydrog Energy 2007;32(14):2957–64.

[47] Tao Y, He Y. Effects of natural convection on latent heat storage performance of salt in a horizontal concentric tube. Appl Energy 2015;143.

[48] Shrivastav AP, Kanti PK, Mohan G, Maiya MP. Design and optimization of metal hydride reactor with phase change material using fin factor for hydrogen storage. J Energy Storage 2024;77.